LA-UR- 09-01612

Approved for public release;
distribution is unlimited.

Title:	Interfacial electron transfer dynamics of Ru(II)-polypyridine sensitized TiO2
Author(s):	E. Jakubikova, R. C. Snoeberger III, V. S. Batista, R. L. Martin, and E. R. Batista
Intended for:	Journal of Physical Chemistry A

Form 836 (7/06)

Interfacial electron transfer dynamics of Ru(II)-polypyridine sensitized TiO_2

Elena Jakubikova, [1] *Robert C. Snoeberger III,* [2] *Victor S. Batista,* [2] *Richard L. Martin,* [1] *and Enrique R. Batista*[*,1]

[1]Theoretical Division, Los Alamos National Laboratory, MS-B268, Los Alamos, NM 87545;

[2]Department of Chemistry, Yale University, P. O. Box 208107, New Haven, CT 06520-8107

[*] Corresponding author. E-mail: erb@lanl.gov

Abstract

Quantum dynamics simulations combined with density functional theory calculations are applied to study interfacial electron transfer (IET) from pyridine-4-phosphonic acid, $[Ru(tpy)(tpy(PO_3H_2))]^{2+}$ and $[Ru(tpy)(bpy)(H_2O)\text{-}Ru(tpy)(tpy(PO_3H_2))]^{4+}$ into the (101) surface of anatase TiO_2. IET rate from pyridine-4-phosphonic acid attached to the nanoparticle in bidentate mode (τ ~ 100 fs) is an order of magnitude faster than the IET rate of the adsorbate attached in the monodentate mode (τ ~ 1 ps). Upon excitation with visible light, $[Ru(tpy)(tpy(PO_3H_2))]^{2+}$ attached to TiO_2 in bidentate binding mode will undergo IET with the rate of ~ 1-10 ps, which is competitive with the excited state decay into the ground state. The probability of electron injection from $[Ru(tpy)(bpy)(H_2O)\text{-}Ru(tpy)(tpy(PO_3H_2))]^{4+}$ is rather low, as the excitation with visible light localizes the excited electron in the tpy-tpy bridge, which does not have favorable coupling with the TiO_2 nanoparticle. The results are relevant to better understanding of the adsorbate features important for promoting efficient interfacial electron transfer into the semiconductor.

Introduction

Ruthenium polypyridyl complexes are a class of compounds displaying rich photophysics and photochemistry, known for their long-lived charge separated excited states.[1] Due to their favorable excited-state properties, they are good candidates in the design of artificial systems capable of converting energy of light into chemical or electrical energy.

For example, ruthenium polypyridyl complexes have been utilized as sensitizers in dye sensitized solar cells.[2-13] They have also been used as chromophores in multi-component molecular assemblies designed to mimic charge transfer events occurring during photosynthesis.[14] Some effort has been devoted to attach such assemblies to the nanocrystalline TiO_2, with the aim to achieve interfacial electron transfer into the semiconductor.[15,16]

Ruthenium polypyridyls have also been used in prototype photocatalytic cells, which would oxidize an organic substrate and produce photocurrent. An example of such assembly consisting of a chromophore-catalyst dyad attached to nanocrystalline TiO_2 was reported by Meyer et al. [17]

In such molecular assemblies on semiconductor surfaces, once the adsorbate molecule is photoexcited, several competing processes can occur: 1. Radiative or nonradiative transition back into the ground state; 2. Intersystem crossing into the lowest triplet excited state; or 3. Interfacial electron transfer into the semiconductor. In the case of ruthenium complexes, such as $[Ru(tpy)_2]^{2+}$, intersystem crossing (IC) will play an important role because the lowest triplet excited states are of metal to ligand charge transfer (MLCT) type with lifetimes of as long as 250 ps at the room temperature.[18] Therefore, the excited states which lead to the electron injection into the semiconductor will be a combination of singlet excited states and a thermalized ^{3}MLCT state.

In this work we study the dynamics of electron injection into the (101) surface of anatase TiO_2 from $[Ru(tpy)_2]^{2+}$ molecule and its complex with the $[Ru(tpy)(bpy)(H_2O)]^{2+}$ catalyst,[19] $[Ru(tpy)(bpy)(H_2O)\text{-}Ru(tpy)_2]^{4+}$. Although the excited state lifetime of $[Ru(tpy)_2]^{2+}$ is shorter than that of other ruthenium polypyridyl compounds,[18] this molecule is often used in molecular assemblies[20] and dye-sensitized solar cells[11,21] due to its advantageous linear directionality. We use a phosphonic acid linker for attachment to TiO_2, since it provides more stable attachment to the semiconductor surface in comparison to other widely used linkers.[22-24]

$Ru(tpy)_2$ attachment to TiO_2 nanoparticles using both carboxylic and phosphonic acids was considered before by Lundqvist et al.[25] In an earlier work they also studied TiO_2 nanoparticles sensitized by pyridine.[26] Persson et al. also performed periodic DFT study of pyridine bound to TiO_2 via carboxylic and phosphonic acid,[27] as well as studies of photoinjection processes in other dye-sensitized TiO_2 nanoparticles.[28-31] The electron injection rates obtained in their work have been estimated from a time-independent picture of the electronic overlap between the adsorbate and nanoparticle orbitals. Our approach to obtaining interfacial electron transfer rates is more direct – employing a quantum dynamics approach, previously used to study electron injection in sensitized TiO_2 semiconductors.[32] The only aspect missing in our approach is electron-phonon coupling.

We study excited state properties of the adsorbates as well as the subsequent interfacial electron transfer from the adsorbates into the semiconductor. Our goal is to gain a better understanding as to which features of the catalyst-chromophore molecular assembly are important for efficient interfacial electron transfer into the semiconductor. We found that while the chromophore by itself injects electrons into TiO_2 on a picoseconds time scale, modifications to the catalyst-chromophore assembly are needed, which would make the tpy-tpy bridging ligand

less electron accepting and thereby favor electron excitations into the tpy(PO_3H_2) ligand directly attached to the nanoparticle.

Methodology

Geometry optimization

The anatase (101) surface of TiO_2 was optimized using Vienna Ab Initio Simulation Package (VASP).[33,34] First, bulk TiO_2 was optimized using periodic boundary conditions (PBC) with PBE exchange-correlation functional[35] along with Projector Augmented-Wave method.[36,37] The energy cutoff of plane wave expansion was set to 400 eV. The TiO_2 unit cell[38] was relaxed using a (13 x 13 x 13) k-point sampling, resulting in the lattice constants a = b = 3.8336 Å and c = 9.6127 Å. Next, the (101) vacuum surface slab was constructed with the depth of approximately 10 Å. The upper layer (top 2 layers of Ti atoms and top 4 layers of O atoms) with pyridine-phosphonic acid attached in mono-dentate and bi-dentate binding mode was re-optimized using (5 x 3 x 1) k-point sampling, keeping the supercell volume fixed (lattice vectors a = 10.3490 Å, b = 15.3344 Å, c = 26.0 Å for bidentate attachment and c = 27.0 Å for monodentate attachment) and the bottom layer frozen.

The geometry of $[Ru(tpy)(tpy(PO_3H))]^{1+}$ and $[Ru(tpy)(bpy)(H_2O)\text{-}Ru(tpy)(tpy(PO_3H))]^{3+}$ adsorbates was optimized using Gaussian 03 computational chemistry package[39] at the PBE0 level of theory,[40] with LANL08 basis set [41,42] on Ru and 6-31G* basis set[43,44] on all other atoms. Phosphonic acid and a portion of the pyridine ring (three carbon atoms) from the pyridine-4-phosphonic acid moiety were kept frozen at the surface configuration during the optimization. The adsorbates were then attached to the surface by overlapping the pyridine-4-phosphonic acid moiety of the optimized adsorbates with the surface-optimized pyridine-4-phosphonic acid.

Finally, the geometry of the free $[Ru(tpy)(tpy(PO_3H_2))]^{2+}$ and $[Ru(tpy)(bpy)(H_2O)$-$Ru(tpy)(tpy(PO_3H_2))]^{4+}$ was optimized in vacuum using the same functional and basis set as described above.

Excited states and absorption spectra

TD-DFT[45-47] with PBE0 functional and basis set as above was employed to calculate singlet excited states in the visible region for $[Ru(tpy)(tpy(PO_3H_2))]^{2+}$ and $[Ru(tpy)(bpy)(H_2O)$-$Ru(tpy)(tpy(PO_3H_2))]^{4+}$. Natural transition orbital analysis[48,49] was used to obtain a representation of virtual and occupied orbitals involved in the electronic transition. Absorption spectra were simulated based on the calculated excitation energies and oscillator strengths, using Gaussian line shape and a half width at half maximum (HWHM) of 0.12 eV. All spectra were normalized so that the absorption maximum is equal to one.

The lowest triplet excited states of $[Ru(tpy)(tpy(PO_3H_2))]^{2+}$ and $[Ru(tpy)(bpy)(H_2O)$-$Ru(tpy)(tpy(PO_3H_2))]^{4+}$ were optimized at the PBE0 level of theory with the same basis set as above. The natural orbital picture[50] was used to determine the character of singly occupied molecular orbitals of the optimized triplet excited states.

Electron transfer dynamics simulations

Electronic structure of the complete nanostructure (adsorbate molecules attached to TiO_2 surface) was obtained using the semi-empirical extended Hückel method (eH). The eH Hamiltonian was used previously for simulations of electron dynamics.[32] Note that while geometry of the TiO_2 nanostructure was optimized in VASP using periodic boundary conditions, PBCs were not used in the electron transfer dynamics simulations.

To study the electron transfer dynamics, one must first solve the stationary Schrödinger equation to obtain molecular orbitals $|q\rangle$ of the initial state $|\Psi(0)\rangle$:

$$\mathbf{H}\mathbf{Q}^q = E_q\mathbf{S}\mathbf{Q}^q \tag{1}$$

Here $\mathbf{H}$ represents the extended Hückel Hamiltonian matrix, $\mathbf{S}$ is the atomic orbital overlap matrix and $\mathbf{Q}^q$, E_q are the corresponding eigenvectors and eigenvalues. Molecular orbitals of the initial state are expressed as

$$|q\rangle = \sum_i Q_i^q |\chi_i\rangle, \tag{2}$$

in which $|\chi_i\rangle$ represent the basis set of the atomic orbitals (AOs). The initial state can be expanded in terms of the molecular orbitals as

$$|\Psi(0)\rangle = \sum_q C_q |q\rangle = \sum_q C_q Q_i^q |\chi_i\rangle, \tag{3}$$

in which C_q are the expansion coefficients. In our simulations, the initial states are defined in terms of the excited electronic states of the adsorbate, which have significant electronic coupling with the semiconductor conduction band (i.e., states in which the excited electron occupies virtual orbitals of the adsorbate positioned within the conduction band).

Next, the initial state $|\Psi(0)\rangle$ is evolved in time to obtain the time-dependent wavefunction:

$$|\Psi(t)\rangle = |\Psi(0)\rangle e^{-(i/\hbar)E_q t} \tag{4}$$

$$|\Psi(t)\rangle = \sum_i \sum_q C_q Q_i^q e^{-(i/\hbar)E_q t} |\chi_i\rangle \tag{5}$$

$$|\Psi(t)\rangle = \sum_i B_i(t)|\chi_i\rangle, \quad B_i(t) = \sum_q C_q Q_i^q e^{-(i/\hbar)E_q t} \tag{6}$$

Finally, one can project time-evolved electronic wavefunction onto the atomic orbitals of the molecular adsorbate to obtain the survival probability $P(t)$:

$$P(t) = \left| \sum_i^{ads.} \sum_j^{all} B_i^*(t) B_j(t) S_{ij} \right|, \tag{7}$$

in which the first summation over i runs through the molecular orbitals of the adsorbate and the second sum over j runs through the molecular orbitals of both the adsorbate and the nanoparticle.

$P(t)$ characterizes the interfacial electron transfer (IET) rate and describes the probability that the photoexcited electron remains in the adsorbate molecule at a time t after the excitation of the system.

IET simulations from pyridine-4-phosphonic acid into TiO_2 were performed using a TiO_2 nanoparticle (lattice vectors a = 10.3490 Å, b = 15.3344 Å, depth ~ 10 Å) optimized in VASP as described above.

In case of the $[Ru(tpy)(tpy(PO_3H_2))]^{2+}$ and $[Ru(tpy)(bpy)(H_2O)\text{-}Ru(tpy)(tpy(PO_3H_2))]^{4+}$, the simulations were conducted on a 3 x 3 adsorbate-anatase supercell array (lattice vectors a = 31.047 Å, b = 46.0032 Å). To avoid artificial recurrences in electron-transient populations, the calculations of charge injection include imaginary absorbing potentials at the boundaries of the supercell. Imaginary potentials were placed on the Ti *d* orbitals, since these are the atomic orbitals which form the conduction band. The value of the absorbing potential was determined by increasing its magnitude until the survival probability converged. For all simulations performed in this work, the value of ~ 0.1/fs was used. No imaginary potentials were used in IET simulations from pyridine-4-phosphonic acid.

Results and Discussion

We start this section with simulations of electron injection from pyridine-4-phosphonic acid attached to the nanoparticle in monodentate and bidentate binding modes. The aim of these simulations is to determine which of the two attachment modes promotes electron injection more readily into TiO_2, and we focus on that type of binding for the subsequent calculations.

Next, we describe IET dynamics from the sensitizer, $[Ru(tpy)(tpy(PO_3H_2))]^{2+}$ and the dyad, $[Ru(tpy)(bpy)(H_2O)\text{-}Ru(tpy)(tpy(PO_3H_2))]^{4+}$, adsorbates attached to a TiO_2 nanoparticle. IET simulations are performed from all adsorbate virtual orbitals localized in the conduction band of

TiO_2. While IET simulations provide us with the electron injection rates from various virtual orbitals, these rates must be weighted with the probability of photoexcitation of an electron to that particular orbital. This information was obtained from TD-DFT calculations. The combination of the results obtained from the IET simulations and TD-DFT calculations allows us to make predictions about the plausibility and rate of the interfacial electron transfer from excited adsorbates into TiO_2.

Electron injection from pyridine

The pyridine-4-phosphonic acid (**1**) can be attached to a TiO_2 nanoparticle in monodentate and bidentate modes (see Figure 1), which are the most stable adsorption modes for the phosphonic acid anchor group.[23]. The binding energies of these two modes differ by only 0.7 kcal/mol, and are essentially identical at the level of theory being considered here. Therefore, both attachments were studied to find the one with lower impedance. The dynamics of electron injection from the lowest unoccupied molecular orbital (LUMO), which corresponds to a π^* orbital localized on pyridine of the pyridine-4-phosphonic acid adsorbate, into the conduction band of TiO_2 is shown in Figure 2.[†] The injection process from pyridine moiety into the TiO_2 nanostructure is an order of magnitude faster in the case of the bidentate binding mode. Electron injection from the LUMO of **1** attached in bidentate mode occurs at the time scale of 100 fs, while the electron injection in the monodentate attachment mode will occur at the time scale of ~ 1 ps. This difference is likely due to the presence of two P-O-Ti bridges in the bidentate binding mode versus one P-O-Ti bridge in the monodentate binding mode, since the electron transfer from adsorbate into the nanoparticle occurs mainly through P-O-Ti bridge. Additionally, the pyridine group in bidentate attachment is rotated by approximately 90° with respect to the phosphonic acid linker in

[†] Imaginary potentials were not used in performing these simulations.

comparison to the pyridine group in monodentate attachment (see Figure 2), which possibly leads to a better orbital overlap and stronger coupling with the nanoparticle. Because of the lower impedance in the bidentate attachment, this mode was chosen for the studies of IET dynamics of $[Ru(tpy)(tpy(PO_3H_2))]^{2+}$ and $[Ru(tpy)(bpy)(H_2O)\text{-}Ru(tpy)(tpy(PO_3H_2))]^{4+}$.

The time scale for IET for monodentate and bidentate attachment of **1** was previously estimated by Nilsing et al. to be 35 fs and 32 fs, respectively.[27] These previous calculations suggest no significant difference between the two linking modes, and they are 1-2 orders of magnitude faster than the electron injection rate predicted by our simulations. The methodology used by Nilsing et al. is intrinsically different from the one reported here. In Nilsing's work, the injection time was estimated in the framework of the density functional theory from the full width at half maximum of the adsorbate DOS once projected onto the surface-adsorbate system (a variation of Newns-Anderson approach[51,52]) making it very difficult to assess the source of the differences in the two predictions.

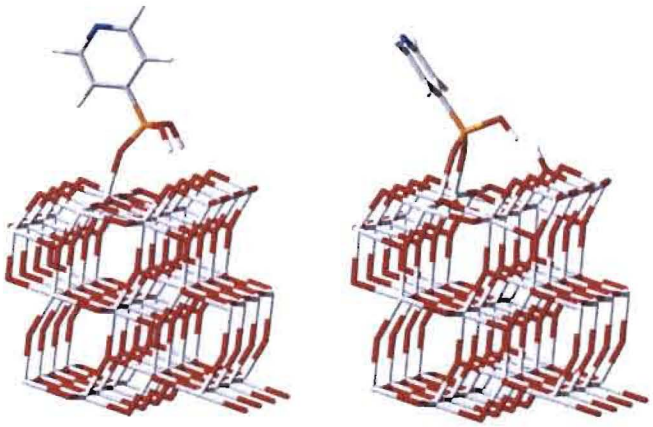

Figure 1. Model nanostructure after geometry relaxation of surface and pyridine-4-phosphonic acid in monodentate and bidentate mode.

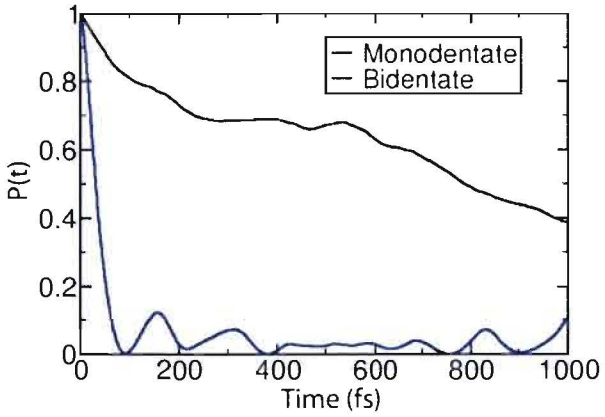

Figure 2. Survival probability for electron relaxation starting from the LUMO orbital of adsorbate for monodentate and bidentate attachment to TiO_2.

Electron injection from the sensitizer $[Ru(tpy)(tpy(PO_3H_2)]^{2+}$

IET simulations

The sensitizer $[Ru(tpy)_2]^{2+}$ was functionalized with a phosphonic acid linker, $[Ru(tpy)(tpy(PO_3H_2))]^{2+}$ (**2**), and attached to the TiO2 nanoparticle in a bidentate mode (see Figure 3). The density of states (DOS) obtained by the extended Hückel (eH) method for **2** adsorbed on TiO_2 is shown in Figure 4. The plot of DOS shows the presence of energy levels from the adsorbate in the bandgap of TiO_2. Additionally, there is a number of virtual orbitals (LUMO through LUMO+13) positioned within the conduction band. These are the adsorbate orbitals that, upon photoexcitation, are responsible for promoting the IET. Virtual molecular orbitals representative of the various types of spatial distribution and symmetry, can be seen in Figure 5.

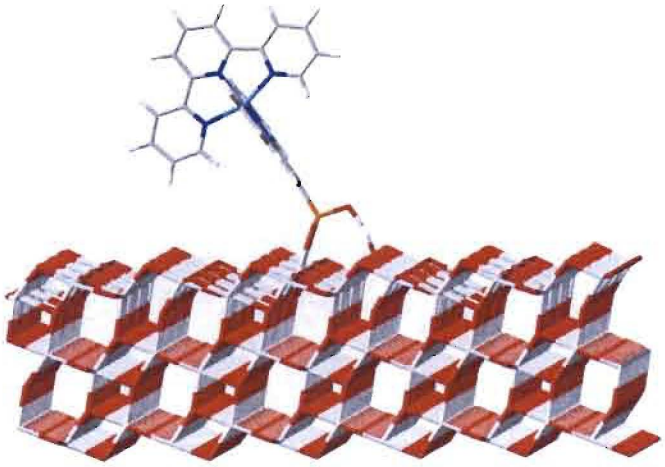

Figure 3. $[Ru(tpy)(tpy(PO_3H_2))]^{2+}$ in the bidentate binding mode on 3x3 slab of TiO_2.

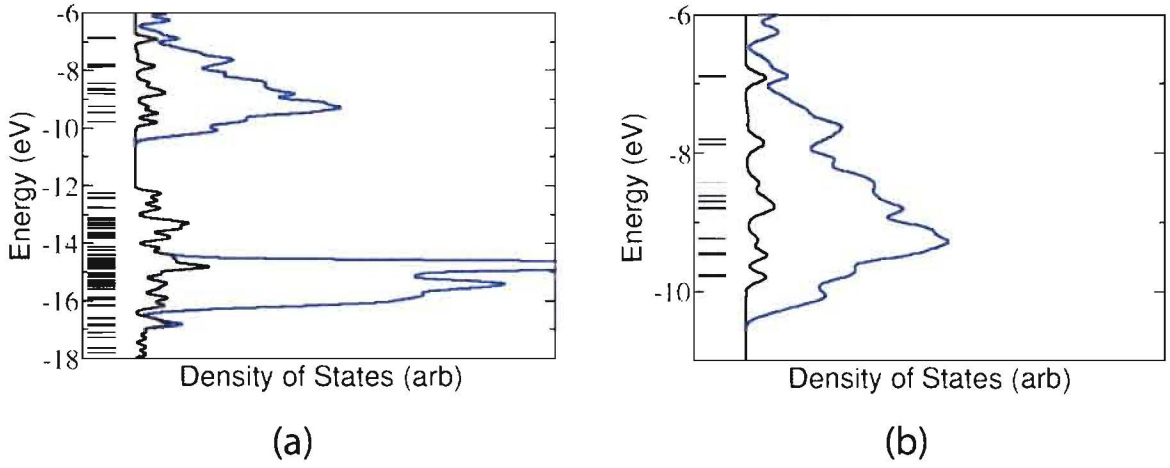

Figure 4. Density of states (DOS) obtained from the extended Hückel method for the $[Ru(tpy)(tpy(PO_3H_2))]^{2+}$-anatase model nanostructure. (a) shows the valence and conduction bands; (b) shows expanded conduction band. In both plots, blue line shows the total DOS and black line represents the projected DOS onto the adsorbate orbitals. The levelset lines give the molecular orbital energies of the free adsorbate in vacuum. DOS is convoluted with a Gaussian function (FWHM = 0.1 eV).

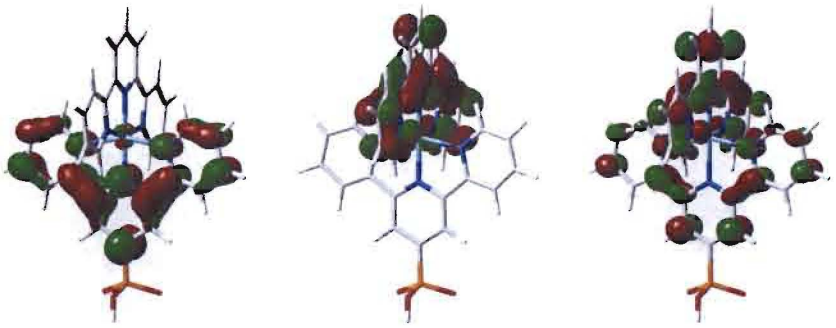

Figure 5. Virtual molecular orbitals obtained from Extended Hückel theory.

Several of the orbitals positioned in the band gap (LUMO, LUMO+2, LUMO+3, LUMO+5, LUMO+7, LUMO+8, LUMO+10 and LUMO+13) have significant electron population on the tpy(PO_3H_2) ligand. These orbitals have relatively strong electronic coupling with the conduction band of TiO_2 and can promote efficient interfacial electron transfer. Ignoring the linker and assuming C_{2v} symmetry for $[Ru(tpy)_2]^{2+}$, LUMO, LUMO+5, and LUMO+10 orbitals belong to *b1* symmetry species, while LUMO+2, LUMO+3, LUMO+7, LUMO+8 and LUMO+13 have *a2* symmetry. Adsorbate orbitals with *b1* symmetry give an IET rate of approximately 1 ps, while those with *a2* symmetry give an IET rate of ~10 ps (see Figure 6). Interestingly, all orbitals have minimal electron population on the phosphonic acid linker. This is probably responsible for the slower IET rate observed for dyes attached to TiO_2 via the phosphonic acid linker compared to the carboxylic acid linker.

Lundqvist et al.[25] estimated the electron injection rate using the Newns-Anderson approach[51,52] from LUMO of **2** into a nanocrystalline TiO_2 to be 65 fs, which is two orders of magnitude faster than the electron injection rate determined by our calculations. As mentioned above, the two methodologies are intrinsically different as the Newns-Anderson approach is based on the orbital overlap for the LUMO of the adsorbate (in terms of the energy shift and broadening) when interacting with the substrate. On the other hand, we have carried out the time evolution of the

initial wavepacket localized on the adsorbate LUMO. Both our and Newns-Anderson approaches do not take into account vibrational effects, Franck-Condon factors and reorganization energies.

Experimental measurements[10] performed on donor-Ru(II) bisterpyridine-phosphonic acid-nanocrystalline TiO_2 assembly suggest that the electron transfer from the terpyridine group attached to the semiconductor is very fast, with the rate < 1 ns which is in agreement with the 1 to 10 ps injection times calculated.

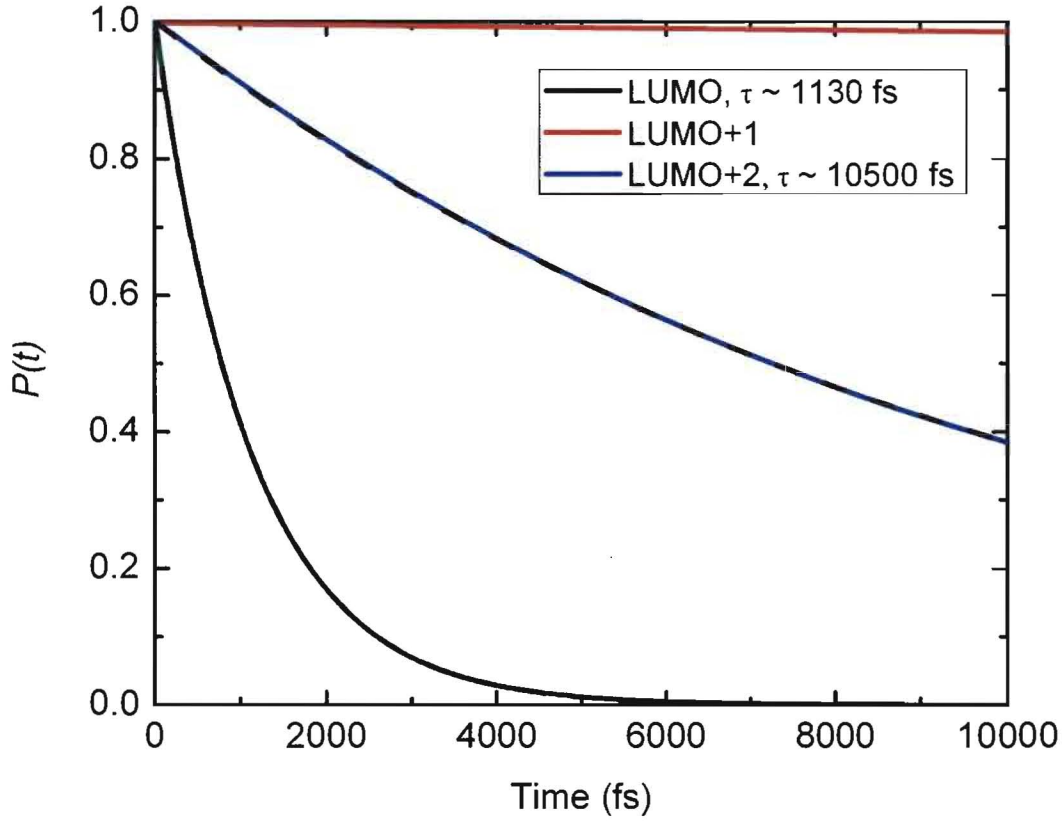

Figure 6. Survival probability for electron relaxation starting from the LUMO, LUMO+1 and LUMO+2 virtual orbitals of $[Ru(tpy)(tpy(PO_3H_2))]^{2+}$ adsorbate. An estimated rate is plotted with the black dashed line.

Our calculations of injection times for the virtual orbitals with the electron population on the second terpyridine ligand not attached to TiO_2 (LUMO+1, LUMO+6, LUMO+11, LUMO+12)

and those with the electron population on Ru *d* orbitlal (LUMO+4 and LUMO+9) indicate that those orbitals either do not inject or the time scale is much slower as no significant adsorbate electron population loss was observed.

States populated upon photoexcitation

The simulated absorption spectrum in the visible region for free $[Ru(tpy)(tpy(PO_3H_2))]^{2+}$, obtained by the TD-DFT formalism, is shown in Figure 7. The shape and the main peaks of the spectra reproduce the experimental data[18] reasonably well, although the peaks are shifted by about 0.5 eV to the higher energies. Such peak shifts are not uncommon for TD-DFT calculations.[53] One should also keep in mind that our calculations were performed in vacuum with the phosphonic acid attached to one of the terpyridine groups, while the experimental data were obtained for $[Ru(tpy)_2]^{2+}$ in solution (acetonitrile), which stabilizes the MLCT excited states and can account for some of the peak shift and slightly different features of the spectra. The most intense peaks, represented by excitations C and D in Figure 7, correspond to the excitation of a particle into the orbitals with electron density on the $tpy(PO_3H_2)$ ligand. Natural transition orbitals (NTOs) corresponding to these excitations are shown in Figure 8. The particle for the excitation C is mainly located on the orbital with *b1* symmetry, which would indicate a possibility of electron injection into the TiO_2 nanoparticle at ~ 1 ps time scale. In the case of excited state D, the particle is mainly located on an orbital which has *a2* symmetry, indicating the time scale for the electron injection in this case to be at the slower, 10 ps timescale. In this line of reasoning, excited state A will inject at the 1 ps timescale and excited state F will inject at 10 ps timescale. Excited states B and E will not lead to the electron injection into TiO_2, since they have no significant population on the $tpy(PO_3H_2)$ ligand.

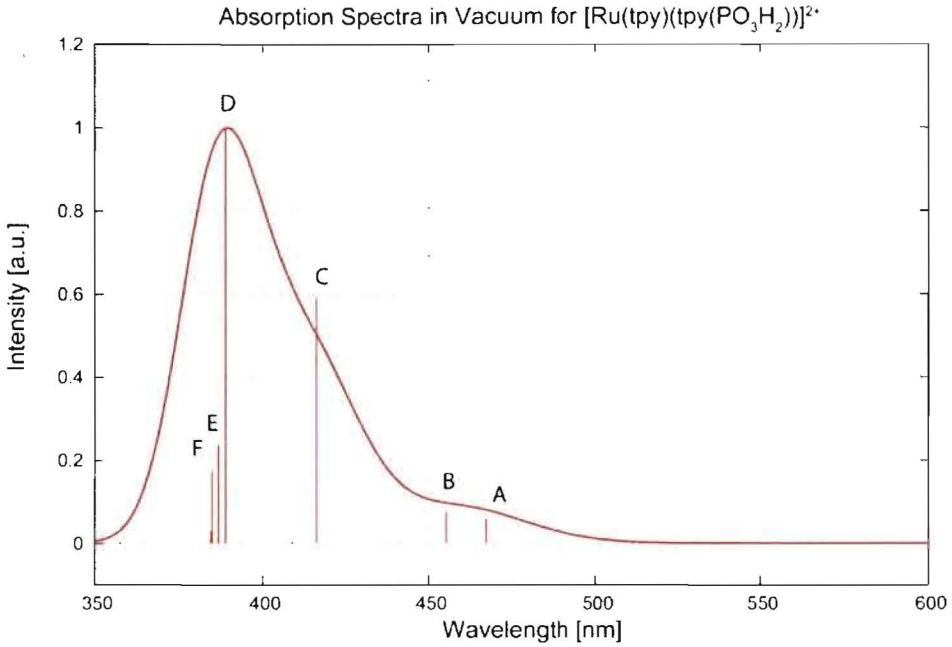

Figure 7. Absorption spectra of $[Ru(tpy)(tpy(PO_3H_2))]^{2+}$ obtained with TD-DFT.

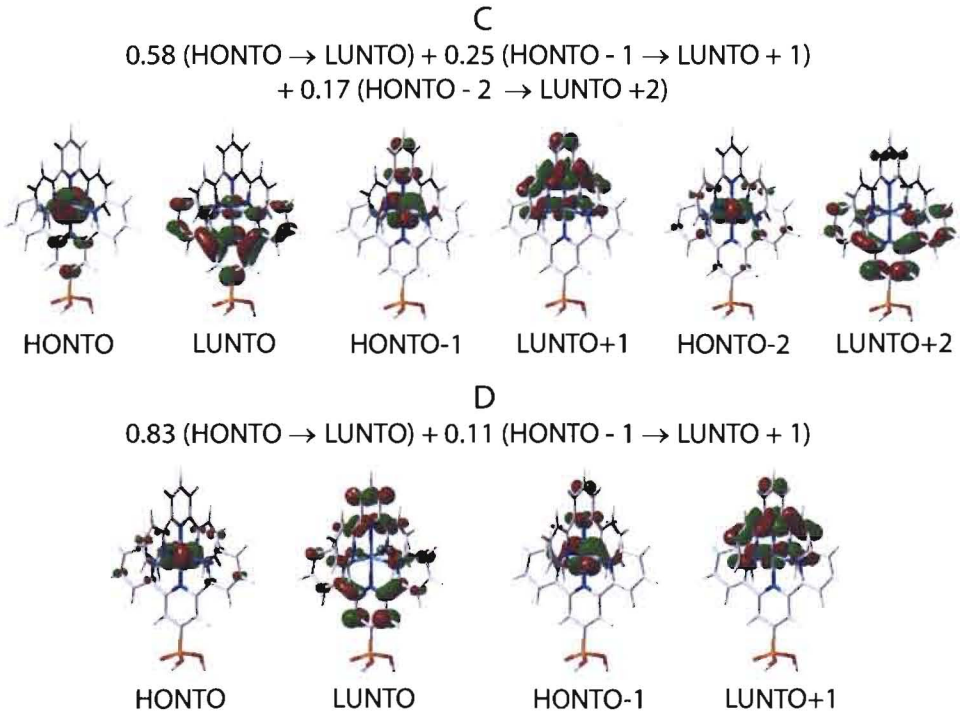

Figure 8. Natural transition orbitals for the most intense excitations of free $[Ru(tpy)(tpy(PO_3H_2))]^{2+}$. Labels C and D correspond to the labeling of absorption peaks in

Figure 7. HONTO stands for the highest occupied natural transition orbital and LUNTO stands for the lowest unoccupied natural transition orbital.

Electron injection from the adsorbate does not need to necessarily occur from the optically active excited states. $[Ru(tpy)_2]^{2+}$ in an excited singlet state can undergo intersystem crossing into the lowest triplet excited state. The two lowest triplet excited states of **2** are shown in Figure 9. Our calculations predict that these two states are very close in the energy, with ^{3}MC (metal centered) state being lower by only 4 kcal/mol. Based on IET simulations, the ^{3}MC state does not lead to the electron injection into TiO_2, while the ^{3}MLCT state will inject an electron into TiO_2 at a 1 ps timescale. Since the emission from the ^{3}MLCT state of $[Ru(tpy)_2]^{2+}$ has been observed experimentally with a lifetime of 250 ps at the room temperature,[18] one would expect this state to be populated in the case of **2** as well. Moreover, since the timescale for the electron injection into TiO_2 is two orders of magnitude smaller than the recombination lifetime, the electron injection will also be competitive with the decay back to the ground state.

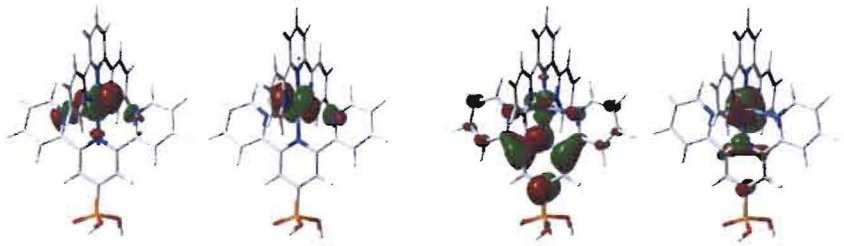

Figure 9. Singly occupied natural orbitals and relative energies of ^{3}MC and ^{3}MLCT states of $[Ru(tpy)(tpy(PO_3H_2))]^{2+}$ optimized in vacuum.

Electron injection from $[Ru(tpy)_2\text{-}Ru(tpy)(bpy)(H_2O)]^{4+}$

IET simulations

Electron injection from $[Ru(tpy)(bpy)(H_2O)\text{-}Ru(tpy)(tpy(PO_3H_2))]^{4+}$ (**3**) into the TiO_2 nanoparticle was studied in the bidentate binding mode (see Figure 10). As in the case of **2**, attachment of **3** to the nanoparticle introduces a number of virtual orbitals (LUMO through LUMO+19) in the conduction band of TiO_2. We have performed simulations of the interfacial electron transfer from each of these virtual orbitals. Some representative virtual molecular orbitals are shown in Figure 11.

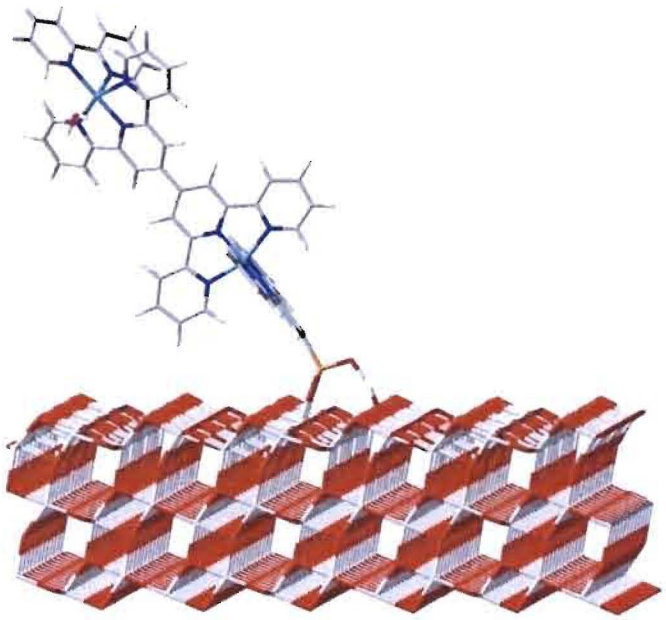

Figure 10. $[Ru(tpy)(bpy)(H_2O)\text{-}Ru(tpy)(tpy(PO_3H_2))]^{4+}$ on a 3x3 slab of TiO_2.

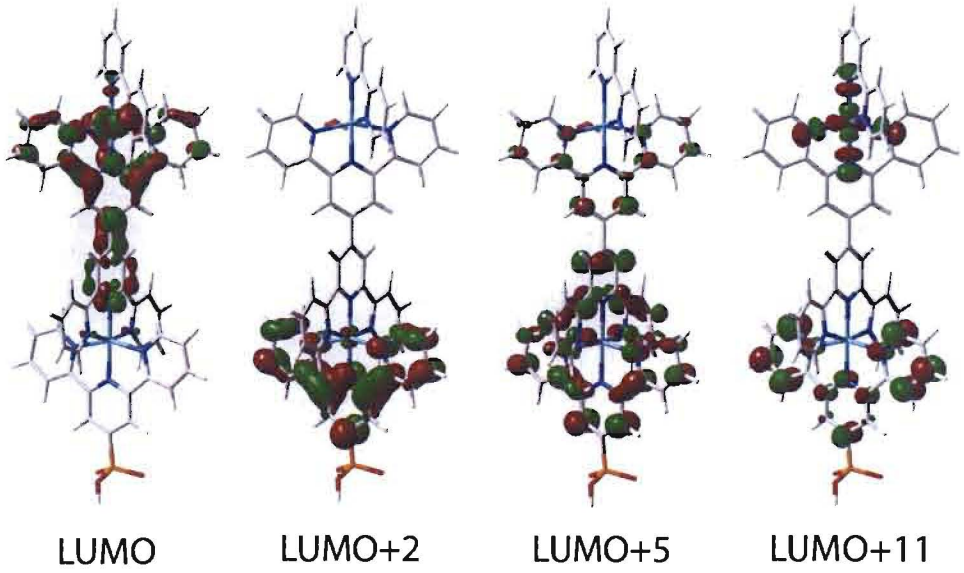

Figure 11. Virtual molecular orbitals of $[Ru(tpy)(bpy)(H_2O)\text{-}Ru(tpy)(tpy(PO_3H_2))]^{4+}$ obtained from the Extended Hückel theory.

Eight of the virtual orbitals positioned in the band gap (LUMO+2, LUMO+5, LUMO+6, LUMO+7, LUMO+11, LUMO+12, LUMO+13, and LUMO+16) have significant electron population on the terpyridine ligand covalently attached to TiO_2 through the phosphonic acid linker. These are the orbitals that promote interfacial electron transfer. Assuming C_{2v} symmetry and ignoring the phosphonic acid linker and the $Ru(tpy)(bpy)(H_2O)$ moiety, virtual orbitals with electron population on the $tpy(PO_3H_2)$ ligand can be again divided into two groups: those which belong to *b1* symmetry (LUMO+2, LUMO+11, LUMO+12) and those with *a2* symmetry (LUMO+5, LUMO+6, LUMO+7, LUMO+13, LUMO+16). Three representative graphs of the electron injection dynamics from the molecular assembly to the TiO_2 surface, are shown in Figure 12. The fastest IET rate, ~ 1ps, is observed for the LUMO+2 orbital. IET rates from orbitals LUMO+11 and LUMO+12 have nonexponential probabilities. This is due to the fact that the electron is delocalized over both $[Ru(tpy)(tpy(PO_3H_2)]^{2+}$ and $[Ru(tpy)(bpy)(H_2O)]^{2+}$ subunits and only the charge density on the terpyridine ligand covalently bound to the nanoparticle

couples with the states in the semiconductor leading to injection (see Figure 12). The rates of electron injection from orbitals belonging to the *a2* symmetry are approximately 7 – 21 ps.

Virtual orbitals with electron population on the tpy-tpy bridge (LUMO, LUMO+1, LUMO+4, LUMO+9), Ru(tpy)(bpy)(H_2O) moiety (LUMO+3, LUMO+14, LUMO+17), or on the *d* orbital of Ru atom in $Ru(tpy)_2$ (LUMO+8, LUMO+18), have no observable adsorbate electron population loss on the 10 ps timescale considered in this work. Interestingly, orbitals with relatively high energy and electron density localized on the tpy-tpy bridge (LUMO+15 and LUMO+19) will inject electron into TiO_2 with the rate of ~ 50 ps.

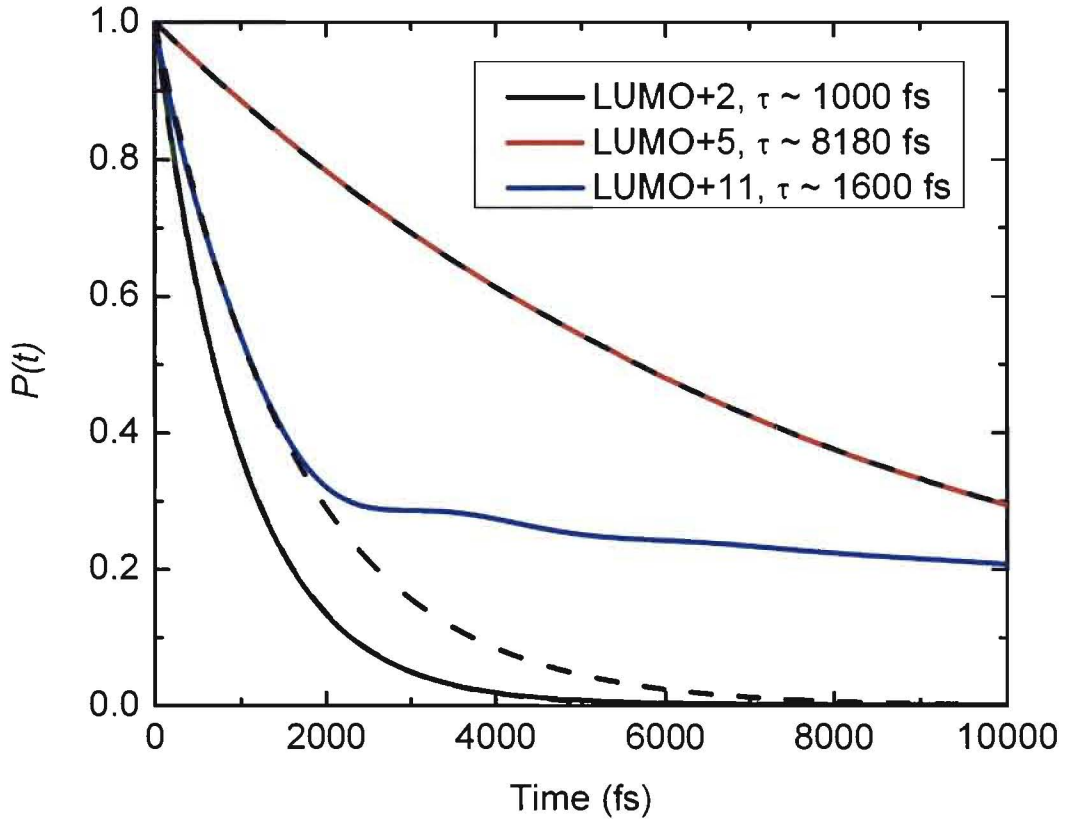

Figure 12. Survival probability for electron relaxation starting from the LUMO+2, LUMO+5, and LUMO+11 virtual orbitals of $[Ru(tpy)(bpy)(H_2O)\text{-}Ru(tpy)(tpy(PO_3H_2))]^{4+}$ adsorbate. An estimated rate is plotted with the black dashed line.

States populated upon photoexcitation

The simulated absorption spectrum for $[Ru(tpy)(bpy)(H_2O)\text{-}Ru(tpy)(tpy(PO_3H_2))]^{4+}$ (**3**) is shown in Figure 13. The two most intense peaks, A and B, correspond to excitations from the ruthenium *d* orbitals, to the bridging tpy-tpy group (see Figure 14). Based on our IET simulations, these excited states will not lead to the electron injection into TiO_2, since they have no significant electron population on the $tpy(PO_3H_2)$ ligand attached to the nanoparticle. Among all other excited states in the visible region, only excitations C, D, and E have significant electron population on the $tpy(PO_3H_2)$ ligand favoring the IET.

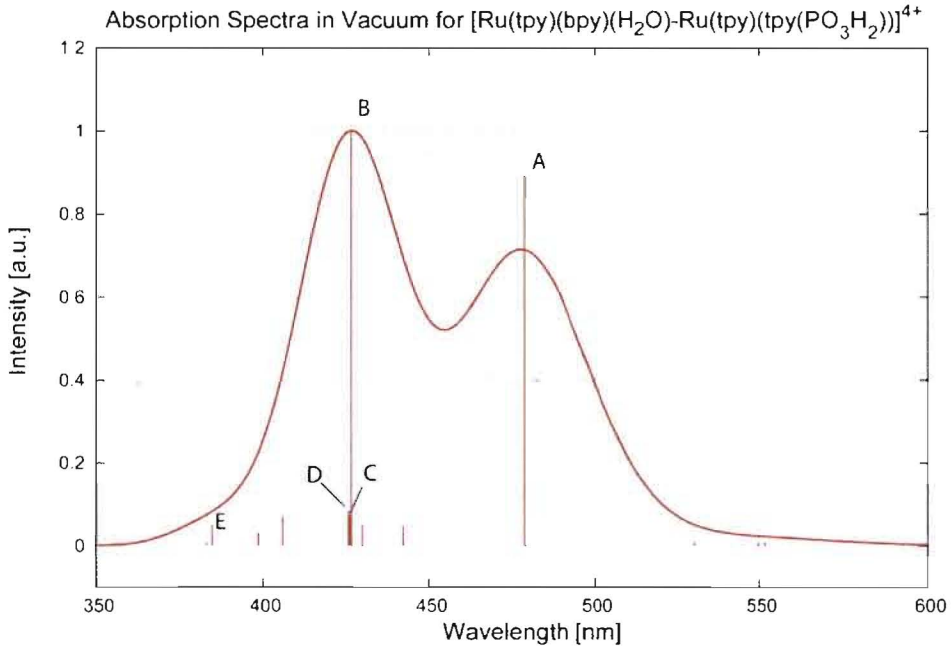

Figure 13. Absorption spectra of $[Ru(tpy)(bpy)(H_2O)\text{-}Ru(tpy)(tpy(PO_3H_2))]^{4+}$ obtained with TD-DFT.

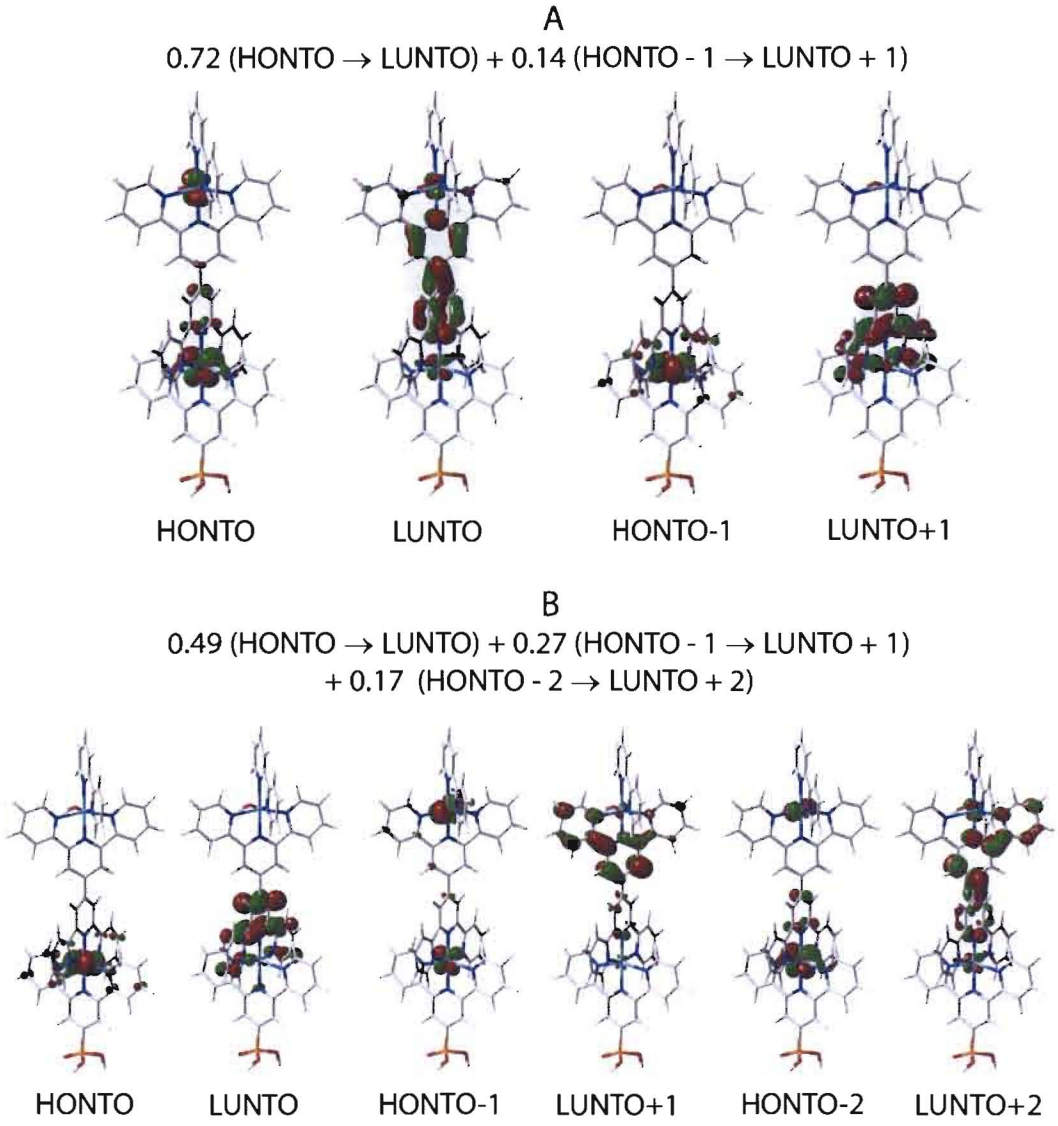

Figure 14. Natural transition orbitals for the most intense excitations of free $[Ru(tpy)(bpy)(H_2O)\text{-}Ru(tpy)(tpy(PO_3H_2))]^{4+}$. Labels A and B correspond to the labeling of absorption peaks in Figure 13. HONTO stands for the highest occupied natural transition orbital and LUNTO stands for the lowest unoccupied natural transition orbital.

As in the case of the $[Ru(tpy)_2]^{2+}$ molecule, $[Ru(tpy)(bpy)(H_2O)\text{-}Ru(tpy)_2]^{2+}$ can also undergo intersystem crossing into the lowest triplet excited state. Singly occupied natural orbitals of the lowest triplet state are shown in Figure 15. Based on our IET simulations this state will not lead

to the electron injection into TiO_2 as there is no significant electron population on the tpy(PO_3H_2) ligand.

Based on the picture of singlet excited states and the lowest triplet excited state of $[Ru(tpy)(bpy)(H_2O)\text{-}Ru(tpy)(tpy(PO_3H_2))]^{4+}$ we suggest that, upon photoexcitation, interfacial electron transfer from the molecular assembly to the semiconductor surface will happen only with low probability. This is the result of the localization of the excited electron in the tpy-tpy bridge, which does not have favorable electronic coupling with the TiO_2 nanoparticle.

It is important to note here that our calculations do not take into account vibrational effects. Therefore, the possibility of the electron injection from the tpy-tpy localized excited state cannot be ruled out as there might be vibrational degrees of freedom coupled to the electron motion through the molecule.

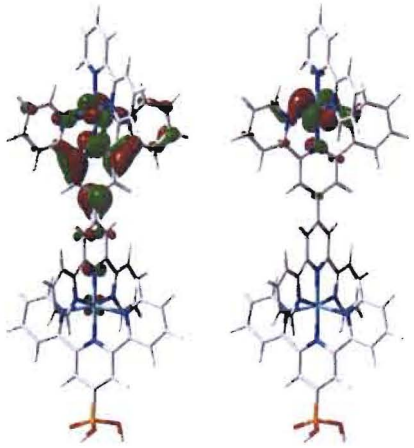

Figure 15. Singly occupied natural orbitals of lowest triplet excited state of $[Ru(tpy)(bpy)(H_2O)\text{-}Ru(tpy)(tpy(PO_3H_2))]^{4+}$ optimized in vacuum.

Conclusions

In this work we have investigated interfacial electron transfer from a series of molecules - pyridine, $[Ru(tpy)_2]^{2+}$, and $[Ru(tpy)_2\text{-}Ru(tpy)(bpy)(H_2O)]^{4+}$, attached to the (101) surface of anatase TiO_2 by the phosphonic acid linker. The IET rates we obtained by doing full quantum

dynamics based on the extended Hückel Hamiltonian are one to two orders of magnitudes slower than those obtained by Newns-Anderson approach.

Simulations of electron injection from pyridine-4-phosphonic acid attached to the anatase TiO_2 showed that the IET is an order of magnitude faster when the phosphonic acid is attached to the surface in bidentate mode. We attribute this to the presence of two P-O-Ti bridges in the bidentate binding mode versus one P-O-Ti bridge in the monodentate binding mode, since the electron transfer from adsorbate into the nanoparticle occurs mainly through P-O-Ti bridge.

Electron injection simulations coupled with the TD-DFT calculations on $[Ru(tpy)(tpy(PO_3H_2))]^{2+}$ suggest that the most intense singlet excited states will undergo IET with the rate of 1 ps or 10 ps, depending on the orbital symmetry of the excited state. Lowest triplet excited state with MLCT character will undergo IET with the rate of ~ 1 ps. This electron injection rate is competitive with the ^{3}MLCT decay into the ground state, which occurs at ~ 250 ps time scale at room temperature.[18] Excited states involving electron excitation into the *d* orbital of Ru or the terpyridine ligand away from the TiO_2 surface will not undergo IET into TiO_2.

The most intense excited states and the lowest triplet excited state of $[Ru(tpy)(bpy)(H_2O)$-$Ru(tpy)(tpy(PO_3H_2))]^{4+}$ will not undergo IET at the timescale considered in this work. This is due to the fact that the excited electron localizes on the tpy-tpy bridge, which does not have favorable coupling with the TiO_2 nanoparticle. This state could, in principle, couple to a more favorable state via phonons. However, one would expect a slower injection rate. Even in the framework of our approximation there is a possibility of the electron injection, albeit with a low probability, as some of the higher excited states with low intensity display significant electron population on the $tpy(PO_3H_2)$ ligand.

These findings have implications for design of artificial photocatalysts, especially when electron injection into the metal oxide semiconductor is desirable. It is important to design molecular assemblies in a way which, upon initial excitation, favors electron localization on the ligands with strong electronic coupling to the semiconductor. In the context of our catalyst-chromophore model system, modifications to tpy-tpy bridging ligand are needed which would make it less electron accepting and thereby favor electron excitations into the tpy(PO_3H_2) ligand. Alternatively, one could substitute electron withdrawing groups directly onto the tpy(PO_3H_2) ligand to achieve favorable electron localization.

Acknowledgements

R. S. thanks Center for Nonlinear Studies at Los Alamos National Laboratory for summer research fellowship. This work was supported by the Laboratory Directed Research and Development (LDRD) program at Los Alamos National Laboratory. Los Alamos National Laboratory is operated by Los Alamos National Security, LLC, for the National Nuclear Security Administration of the U.S. Department of Energy under contract DE-AC52-06NA25396.

References

(1) Roundhill, D. M. Photochemistry, photophysics, and photoredox reactions of $Ru(bpy)_3^{2+}$ and related complexes. In *Photochemistry and photophysics of metal complexes*; Plenum Press: New York, 1994; pp 165.

(2) Bach, U.; Lupo, D.; Comte, P.; Moser, J. E.; Weissortel, F.; Salbeck, J.; Spreitzer, H.; Gratzel, M. *Nature* 1998, *395*, 583.

(3) Hagfeldt, A.; Gratzel, M. *Chem. Rev.* 1995, *95*, 49.

(4) O'Regan, B.; Gratzel, M. *Nature* 1991, *353*, 737.

(5) Zakeeruddin, S. M.; Nazeeruddin, M. K.; Pechy, P.; Rotzinger, F. P.; HumphryBaker, R.; Kalyanasundaram, K.; Gratzel, M.; Shklover, V.; Haibach, T. *Inorg. Chem.* 1997, *36*, 5937.

(6) Argazzi, R.; Bignozzi, C. A.; Heimer, T. A.; Castellano, F. N.; Meyer, G. J. *J. Am. Chem. Soc.* 1995, *117*, 11815.

(7) Argazzi, R.; Bignozzi, C. A.; Heimer, T. A.; Castellano, F. N.; Meyer, G. J. *J. Phys. Chem. B* 1997, *101*, 2591.

(8) Islam, A.; Sugihara, H.; Arakawa, H. *J. Photochem. Photobiol., A* 2003, *158*, 131.

(9) Katoh, R.; Furube, A.; Kasuya, M.; Fuke, N.; Koide, N.; Han, L. *J. Mater. Chem.* 2007, *17*, 3190.

(10) Bonhote, P.; Moser, J. E.; Humphry-Baker, R.; Vlachopoulos, N.; Zakeeruddin, S. M.; Walder, L.; Gratzel, M. *J. Am. Chem. Soc.* 1999, *121*, 1324.

(11) Beley, M.; Bignozzi, C. A.; Kirsch, G.; Alebbi, M.; Raboin, J. C. *Inorg. Chim. Acta* 2001, *318*, 197.

(12) Duprez, V.; Biancardo, M.; Krebs, F. C. *Sol. Energy Mater. Sol. Cells* 2007, *91*, 230.

(13) Figgemeier, E.; Aranyos, V.; Constable, E. C.; Handel, R. W.; Housecroft, C. E.; Risinger, C.; Hagfeldt, A.; Mukhtar, E. *Inorg. Chem. Commun.* 2004, *7*, 117.

(14) Falkenstrom, M.; Johansson, O.; Hammarstrom, L. *Inorg. Chim. Acta* 2007, *360*, 741.

(15) Ghanem, R.; Xu, Y. H.; Pan, J.; Hoffmann, T.; Andersson, J.; Polivka, T.; Pascher, T.; Styring, S.; Sun, L. C.; Sundstrom, V. *Inorg. Chem.* 2002, *41*, 6258.

(16) Wolpher, H.; Sinha, S.; Pan, J. X.; Johansson, A.; Lundqvist, M. J.; Persson, P.; Lomoth, R.; Bergquist, J.; Sun, L. C.; Sundstrom, V.; Akermark, B.; Polivka, T. *Inorg. Chem.* 2007, *46*, 638.

(17) Treadway, J. A.; Moss, J. A.; Meyer, T. J. *Inorg. Chem.* 1999, *38*, 4386.

(18) Sauvage, J. P.; Collin, J. P.; Chambron, J. C.; Guillerez, S.; Coudret, C.; Balzani, V.; Barigelletti, F.; Decola, L.; Flamigni, L. *Chem. Rev.* 1994, *94*, 993.

(19) Moyer, B. A.; Thompson, M. S.; Meyer, T. J. *J. Am. Chem. Soc.* 1980, *102*, 2310.

(20) Han, F. S.; Higuchi, M.; Kurth, D. G. *J. Am. Chem. Soc.* 2008, *130*, 2073.

(21) Houarner-Rassin, C.; Chaignon, F.; She, C.; Stockwell, D.; Blart, E.; Buvat, P.; Lian, T.; Odobel, F. *J. Photochem. Photobiol., A* 2007, *192*, 56.

(22) Gillaizeau-Gauthier, I.; Odobel, F.; Alebbi, M.; Argazzi, R.; Costa, E.; Bignozzi, C. A.; Qu, P.; Meyer, G. J. *Inorg. Chem.* 2001, *40*, 6073.

(23) Nilsing, M.; Lunell, S.; Persson, P.; Ojamae, L. *Surf. Sci.* 2005, *582*, 49.

(24) Pechy, P.; Rotzinger, F. P.; Nazeeruddin, M. K.; Kohle, O.; Zakeeruddin, S. M.; HumphryBaker, R.; Gratzel, M. *J. Chem. Soc., Chem. Commun.* 1995, 65.

(25) Lundqvist, M. J.; Nilsing, M.; Lunell, S.; Akermark, B.; Persson, P. *J. Phys. Chem. B* 2006, *110*, 20513.

(26) Lundqvist, M. J.; Nilsing, M.; Persson, P.; Lunell, S. *Int. J. Quantum Chem.* 2006, *106*, 3214.

(27) Nilsing, M.; Persson, P.; Ojamae, L. *Chem. Phys. Lett.* 2005, *415*, 375.

(28) Persson, P.; Bergstrom, R.; Lunell, S. *J. Phys. Chem. B* 2000, *104*, 10348.

(29) Persson, P.; Lundqvist, M. J. *J. Phys. Chem. B* 2005, *109*, 11918.

(30) Persson, P.; Lundqvist, M. J.; Ernstorfer, R.; Goddard, W. A.; Willig, F. *J. Chem. Theory Comput.* 2006, *2*, 441.

(31) Persson, P.; Lunell, S.; Ojamae, L. *Chem. Phys. Lett.* 2002, *364*, 469.

(32) Rego, L. G. C.; Batista, V. S. *J. Am. Chem. Soc.* 2003, *125*, 7989.

(33) Kresse, G.; Furthmüller, J. *Phys. Rev. B* 1996, *54*, 11169.

(34) Kresse, G.; Furthmüller, J. *Comput. Mater. Sci.* 1996, *6*, 15.

(35) Perdew, J. P.; Burke, K.; Ernzerhof, M. *Phys. Rev. Lett.* 1996, *77*, 3865.

(36) Blöchl, P. E. *Phys. Rev. B* 1994, *50*, 17953.

(37) Kresse, G.; Joubert, D. *Phys. Rev. B* 1999, *59*, 1758.

(38) Djerdj, I.; Tonejc, A. M. *J. Alloys Compd.* 2006, *413*, 159.

(39) Frisch, M. J.; Trucks, G. W.; Schlegel, H. B.; Scuseria, G. E.; Robb, M. A.; Cheeseman, J. R.; Montgomery, J. A.; Vreven, J., T. ; Kudin, K. N.; Burant, J. C.; Millam, J. M.; Iyengar, S. S.; Tomasi, J.; Barone, V.; Mennucci, B.; Cossi, M.; Scalmani, G.; Rega, N.; Petersson, G. A.; Nakatsuji, H.; Hada, M.; Ehara, M.; Toyota, K.; Fukuda, R.; Hasegawa, J.; Ishida, M.; Nakajima, T.; Honda, Y.; Kitao, O.; Nakai, H.; Klene, M.; Li, X.; Knox, J. E.; Hratchian, H. P.; Cross, J. B.; Bakken, V.; Adamo, C.; Jaramillo, J.; Gomperts, R.; Stratmann, R. E.; Yazyev, O.; Austin, A. J.; Cammi, R.; Pomelli, C.; Ochterski, J. W.; Ayala, P. Y.; Morokuma, K.; Voth, G. A.; Salvador, P.; Dannenberg, J. J.; Zakrzewski, V. G.; Dapprich, S.; Daniels, A. D.; Strain, M. C.; Farkas, O.; Malick, D. K.; Rabuck, A. D.; Raghavachari, K.; Foresman, J. B.; Ortiz, J. V.; Cui, Q.; Baboul, A. G.; Clifford, S.; Cioslowski, J.; Stefanov, B. B.; Liu, G.; Liashenko, A.; Piskorz, P.; Komaromi, I.; Martin, R. L.; Fox, D. J.; Keith, T.; Al-Laham, M. A.; Peng, C. Y.; Nanayakkara, A.; Challacombe, M.; Gill, P. M. W.; Johnson, B.; Chen, W.; Wong, M. W.; Gonzalez, C.; Pople, J. A. Gaussian 03; Revision D.02 ed.; Gaussian, Inc.: Wallingford, CT, 2004.

(40) Ernzerhof, M.; Scuseria, G. E. *J. Chem. Phys.* 1999, *110*, 5029.

(41) Hay, P. J.; Wadt, W. R. *J. Chem. Phys.* 1985, *82*, 270.

(42) Roy, L. A.; Hay, P. J.; Martin, R. L. *J. Chem. Theory Comput.* 2008, *4*, 1029.

(43) Hehre, W. J.; Ditchfield, R.; Pople, J. A. *J. Chem. Phys.* 1972, *56*, 2257.

(44) Harihara, P. C.; Pople, J. A. *Theor. Chim. Acta* 1973, *28*, 213.

(45) Bauernschmitt, R.; Ahlrichs, R. *Chem. Phys. Lett.* 1996, *256*, 454.

(46) Casida, M. E.; Jamorski, C.; Casida, K. C.; Salahub, D. R. *J. Chem. Phys.* 1998, *108*, 4439.

(47) Stratmann, R. E.; Scuseria, G. E.; Frisch, M. J. *J. Chem. Phys.* 1998, *109*, 8218.

(48) Martin, R. L. *J. Chem. Phys.* 2003, *118*, 4775.

(49) Batista, E. R.; Martin, R. L. Natural Transition Orbitals. In *Encyclopedia of Computational Chemistry*, 2004.

(50) Davidson, E. R. *Rev. Mod. Phys.* 1972, *44*, 451.

(51) Muscat, J. P.; Newns, D. M. *Prog. Surf. Sci.* 1978, *9*, 1.

(52) Anderson, P. W. *Phys. Rev.* 1961, *124*, 41.

(53) Rappoport, D.; Furche, F. Excited States and Photochemistry. In *Time-Dependent Density Functional Theory*, 2006; pp 337.